This article has been accepted for publication in a future issue of this journal, but has not been fully edited. Content may change prior to final publication. Citation information: DOI 10.1109/TMECH.2019.2951308, IEEE/ASME Transactions on Mechatronics

FlexLab and LevLab: A Portable Control and Mechatronics Educational System

Lei Zhou*, Jun Young Yoon*, Alex Andriën, Mohammad Imani Nejad, Blair T. Allison, and David L. Trumper, *Member, IEEE*

***Abstract*—This paper describes a compact, low-cost, single-board FlexLab/LevLab electromechanical system for use in teaching modeling, dynamics, and control of mechatronic systems. The portable educational platform proposed in this paper enables a *flipped-lab* approach where students can do experimental work outside a dedicated lab facility and so achieve a better understanding through more extensive hands-on experiences. The system has actuators, sensors, and power electronics implemented on a 70 mm × 100 mm printed circuit board (PCB). Mechanical motion in up to three degrees-of-freedom (DOFs) is implemented using on-board spiral coils as Lorentz actuators to drive moving permanent magnets (PM) with Hall effect position sensing on each magnet. The maximum magnet motion range is 4 mm and 3 mm in the vertical direction for the FlexLab and LevLab, respectively, and the positioning noise of the Hall effect sensors with an over-sampling filter is approximately 0.2 μm RMS. In the FlexLab configuration, up to three PM disk pairs can be mounted on a flexible cantilever beam in locations which interact with three spiral coils. This configuration allows modeling, measurement, and control of second-, fourth-, and sixth-order mass-spring system dynamics. In the LevLab configuration, the board can implement both single- and three-DOF magnetic suspension systems via Lorentz forces on either a spherical PM or three pairs of disk PMs on a triangular backbone.**

***Index Terms*—cantilever beam, hands-on education, magnetic levitation, portable educational system**

I. Introduction

A major challenge in teaching control systems and mechatronics is to offer students hands-on experiences, which are essential for students to obtain a fundamental understanding of key phenomena, design methods, and experimental skills. However, in many circumstances, limited lab resources and concentrated lab hours of classes may limit the depth of such knowledge that students can obtain. To address this challenge, we have designed a series of portable educational labs for dynamic systems and control teaching [1]. The vision is that by making the educational mechatronic system portable and lending the hardware to students, they can work on the lab assignments outside the structured lab time, and therefore achieve a better understanding of the subject through hands-on experiences. This requires the mechatronic systems to be low-cost, portable, robust, and able to demonstrate fundamental time- and frequency-domain system responses in a clear fashion.

Over the years, researchers and educators have put a lot of effort in designing educational systems for dynamics and control teaching [2]–[6]. With the advance of embedded system technology, microcontrollers have become powerful enough to provide real-time control performance to many mechatronic systems. Recent works [7], [8] have developed a series of compact teaching labs using embedded real-time micro-controllers that allow at-home lab experiences. This trend of portable labs is also suitable in designing content for Massive Open Online Courses (MOOC).

This paper introduces the design, modeling, and control of the FlexLab/LevLab, which is a complete portable mechatronic system on a single PCB of 70 mm × 100 mm, with a total cost per system of about 70 US dollars in quantity in April, 2018. The FlexLab/LevLab system works together with a myRIO real-time controller from National Instruments [9]. In the FlexLab configuration, an I-shaped or a T-shaped flexible cantilever beam with disk-shaped PMs on the tip is anchored to the PCB with two small bolts at its base. Fig. 1a shows a photograph of the FlexLab with T-shaped beam and two pairs of PMs, which implements a fourth-order dynamic system. Here the PM pairs are clamped to the beam via magnetic attraction. Actuating forces are applied to the beam through the interactions between the PM and actuator coils in the PCB. Linear power amplifiers with a bridge circuit configuration are used to drive the actuator coils. The system can also work with an I-shaped beam using the coil along the beam centerline on the PCB, which implements a second-order dynamic system.

The LevLab configuration implements a magnetic suspension system using the same actuators and sensors. Here, a triangular target with three pairs of PMs is levitated underneath the PCB, as shown in Fig. 1b. The system can also levitate a spherical PM using one coil to

* Both authors equally contributed to this manuscript. (*Corresponding author: Jun Young Yoon.*)

L. Zhou and D. Trumper are with the Department of Mechanical Engineering, Massachusetts Institute of Technology, Cambridge, MA, USA. (e-mail: leizhou@mit.edu, trumper@mit.edu)

J. Y. Yoon is with the School of Mechanical Engineering, Yonsei University, Seoul 03722, South Korea (e-mail: junyoung.yoon@yonsei.ac.kr).

A. Andriën is with the Faculty of Mechanical Engineering, Eindhoven University of Technology, Eindhoven, The Netherlands. (e-mail: A.R.P.Andrien@tue.nl)

M. Imani Nejad is with IIMANII, Inc., Cambridge, MA, USA. (e-mail: imanmamed@gmail.com)

B. Allison is with the Department of Mechanical Engineering, Grove City Collage, Grove City, Pennsylvania, USA. (e-mail: allisonbt@gcc.edu)

This article has been accepted for publication in a future issue of this journal, but has not been fully edited. Content may change prior to final publication. Citation information: DOI 10.1109/TMECH.2019.2951308, IEEE/ASME Transactions on Mechatronics

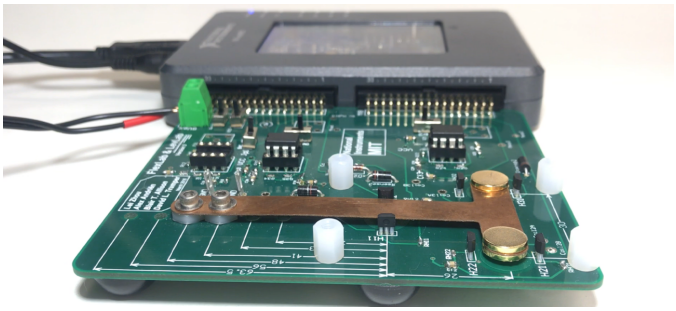

(a)

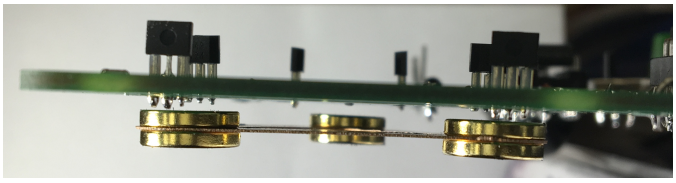

(b)

Fig. 1. (a) Photograph of the 2-DOF FlexLab system attached to myRIO controller. (b) Photograph of the LevLab experiment in operation for 3-DOF levitation.

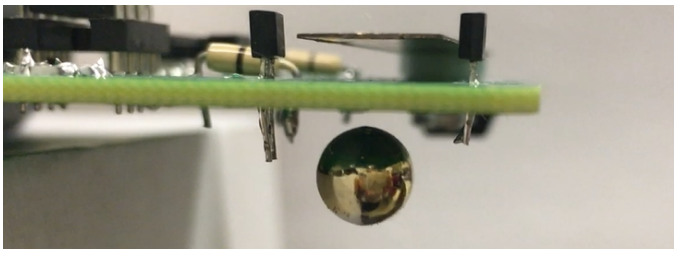

Fig. 2. Photograph of single-DOF magnetic suspension using one coil and a spherical PM.

demonstrate single-DOF magnetic suspension, as shown in Fig. 2. Note that such magnetic levitation technique is widely used for precision system applications discussed in [10], [11]. the portable educational system allows students to work on assignments outside a formal lab facility, and thereby to have more experiences which connect theory with practice in modeling, dynamics, and control of mechatronic systems. The portable FlexLab/LevLab platform with several other educational systems [3]–[6], [8] are compared in terms of cost and device volume as shown in Fig. 3. The comparison shows that the FlexLab/LevLab system is significantly compact in size with relatively low cost, which can be attractive for various educational purposes.

The remainder of this paper is organized as follows: Section II presents the hardware design of the FlexLab and LevLab configurations. Section III then presents the modeling and system identification for both systems. Control system design and control performance are shown in Section IV, and conclusions are presented in Section VI.

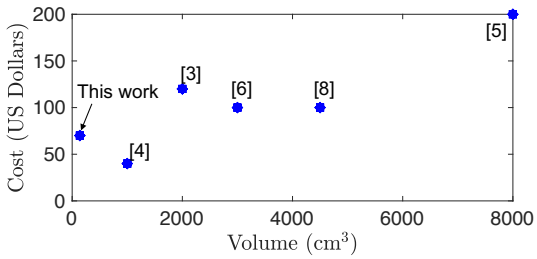

Fig. 3. Comparison of the portable FlexLab/LevLab platform with other educational systems in literature [3]–[6], [8] in terms of cost and device volume.

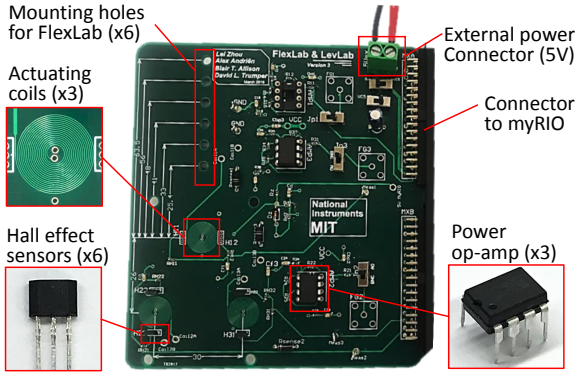

Fig. 4. Photograph of the printed circuit board (PCB) for the FlexLab and LevLab systems with call-outs for major components.

II. Hardware Configuration

A. Printed Circuit Board

Fig. 4 shows the PCB in the FlexLab/LevLab system, which includes the actuator coils, power operational amplifiers, and Hall effect displacement sensors. Note the multiple mounting holes to allow cantilever beams with different length and shape to be used in the FlexLab system.

The actuator coils are three spiral coils formed with PCB traces and using through-hole interconnects between the layers. Each coil has 80 turns, with 4 layers in total and 20 turns per layer. The resistance and the inductance of the coils are 10.5 Ω and 24 μH, respectively. Note that the through-holes were made with larger than minimum diameter, as earlier prototypes had excess coil resistance associated with smaller through holes.

Linear power amplifiers are used in the FlexLab/LevLab to avoid switching noise which might interfere with sensor signals. In our design, the dual power operational amplifier chip TCA0372 from On Semiconductor^{TM} [12] is used. The amplifiers are supplied with 5 V from either the myRIO 5V power supply or from a higher-current external power supply as selected by a switch on the PCB.

Each coil is driven by two amplifiers in a bridge configuration as shown in Fig. 5a. The voltage command signal is V_{in}, which is generated by the real-time controller. The amplifier gain is set to unity by selecting $R_1 = R_2$ and $R_3 = R_4$. The reference voltage V_{ref} is set to 2.35 V,

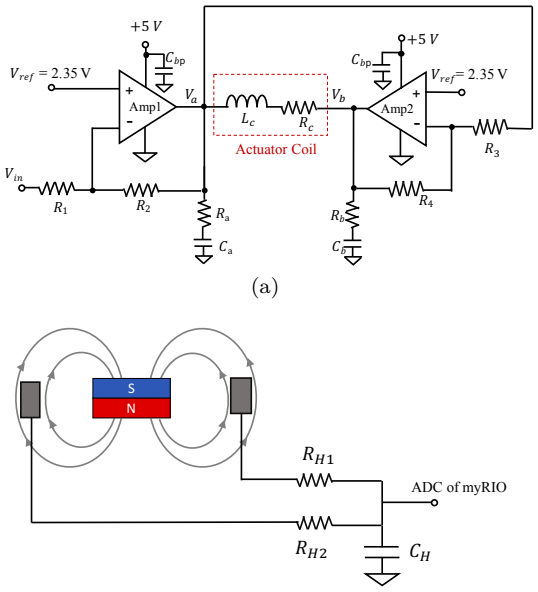

Fig. 5. Circuit diagram of FlexLab/LevLab PCB. (a) Circuit diagram of the power operational amplifiers for actuator coils. Here $V_{ref} = 2.35$ V establishes the balanced bridge reference voltage for the amplifiers. The control signal from the analog output of the myRIO controller is V_{in}. Each amplifier gain is selected to be unity with $R_1 = R_2$ and $R_3 = R_4$. Snubber pairs R_a, C_a and R_b, C_b are included for output stage stability of the amplifiers. In our implementation, $R_a = R_b = 220\ \Omega$, and $C_a = C_b = 0.1\ \mu$F. C_{bp} is the by-pass capacitor for amplifier's power supply. (b) Diagram for Hall effect sensor configuration and circuit.

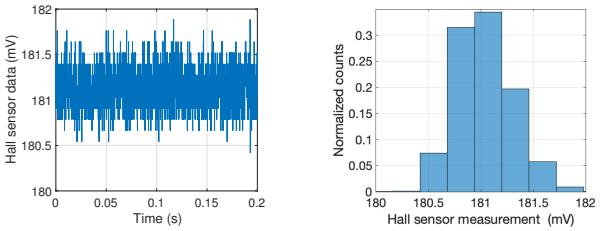

Fig. 6. Noise level of the Hall effect sensor measurement. (a) Time-Voltage data. (b) Histogram. The standard deviation is 0.25 mV, which corresponds to a displacement of about 0.2 μm.

which is about the center of the 0-5 V range. The resistor-capacitor pairs R_a, C_a and R_b, C_b are added to the circuit to suppress an observed amplifier output stage oscillation at about 10 MHz. In our implementation, the values are experimentally selected as $R_a = R_b = 220\ \Omega$, and $C_a = C_b = 0.1\ \mu$F. With a 5 V supply, the output range of the amplifiers lies within about 1–4 V relative to board common. With the circuit shown in Fig. 5a, the voltage across the coil is then $V_c = V_b - V_a = 2V_{in} - 2V_{ref}$, ranging from -3V to +3V.

To measure the vertical displacements of the PMs in the system, two Hall effect sensors (SS49E from Honeywell Inc.) are configured on the sides of each PM with their sensitive directions pointing opposite direction to each other and perpendicular to the PM magnetization direction, as shown in Fig. 5b. This configuration rejects common-mode magnetic fields from external sources, and improves the

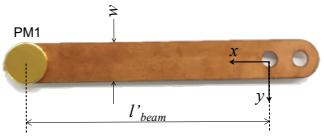

Fig. 7. Photo of I-shaped flexible cantilever beam for FlexLab.

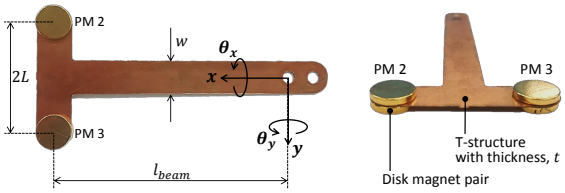

Fig. 8. Photos of T-shaped flexible cantilever beam for FlexLab. (a) Top view with coordinates and geometric parameters definition. (b) Side view of the T-shaped beam showing the disk magnet pairs, which are self-clamped on the beam via magnetic attraction.

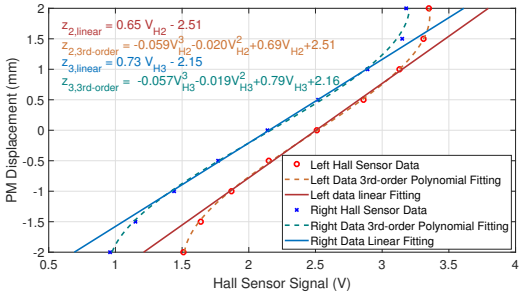

Fig. 9. T-beam FlexLab configuration calibration data for Hall effect sensors output V_{Hj} to PM displacements z_j, and their linear and 3rd-order polynomial fittings. Distance scale is defined to be zero when magnet is centered between the Hall sensors, and increases as magnet moves upward away from PC board. Calibration is based upon moving the magnet with a screw.

sensor sensitivity with respect to the magnet displacement. The bandwidth of the selected Hall effect sensor is 55 kHz. The signals from the two Hall effect sensors are averaged and low-pass filtered through a resistor-capacitor circuit, and are then input to the A/D converter of the myRIO. Here $R_{H1} = R_{H2} = 470\ \Omega$, and $C_H = 0.1\ \mu$F. The noise level of the measurements is limited by the quantization noise of the 12-bit A/D converters. To further reduce the noise level in the measurement, the sensor signals can be over-sampled at 40 kHz in the FPGA, with every 10 samples averaged into one measurement in the control loop running at 4 kHz. Fig. 6 shows the measured Hall effect sensor output data and its histogram after such oversampling. The standard deviation of the measurement is 0.25 mV.

Note that the myRIO by National Instruments is used in this work as a real-time controller for the FlexLab and LevLab system. The associated printed circuit board (PCB) can be readily used with any other real-time microcontrollers (e.g. Arduinos). For such use, the connector between the PCB and the myRIO needs to be adapted to be able to connect to other microcontrollers. In addition, in our current setup, the myRIO is also working as a

This article has been accepted for publication in a future issue of this journal, but has not been fully edited. Content may change prior to final publication. Citation information: DOI 10.1109/TMECH.2019.2951308, IEEE/ASME Transactions on Mechatronics

TABLE I
DESIGN PARAMETERS OF THE FLEXLAB/LEVLAB SYSTEMS.

Description	Parameter	Value
T-shaped Cantilever beam length	l_{beam}	65 mm
T-shaped Cantilever beam width	w	9.525 mm
T-shaped Cantilever beam thickness	t	0.25 mm
Length of connecting bar	$2L$	30 mm
Elastic modulus of beam material	E	110.3 GPa
Shear modulus of beam material	G	38 GPa
Mass of disk magnets on one side	m	1.7 g
Mass of the T-shaped bronze beam	m_{beam}	1.4 g
Amplifier gain	g_{amp}	2 V/V
Resistance of the coil	R_c	10.5 Ω
Distance of magnets in LevLab target	b	30 mm
Geometric parameter of LevLab target	h	26 mm
Mass of the LevLab target assembly	m_{lev}	7.2 g

mechanical fixture for the FlexLab/LevLab system as shown in Fig. 1a. When using other microcontrollers, an additional mechanical support might be needed.

B. Flexible Beam System: FlexLab

The FlexLab system can use an I-shaped cantilever beam with a single magnet pair moving in one DOF, or a T-shaped cantilever beam with two or three magnet pairs moving in two or three DOFs. The I-shaped beam with single pair of magnets is shown in Fig. 7, and the two-magnet configuration with T-shaped beam is shown in Fig. 8. A third PM pair can be added to the T-beam to interact with the coil along the beam centerline. Both beams are water-jet cut from grade 510 bronze shim stock of 0.01 inch thickness. Other thicknesses and geometric configurations can be readily fabricated by users as long as the drive magnets are located in alignment with the on-board coils. Note that in the FlexLab system, the displacement direction for the magnets are in the z-direction, which is pointing upward in the vertical direction. The beam is plastically bent upward by hand after assembling to the PCB such that the the weight of the PMs is compensated by the beam bias force. This establishes a desired nominal gap between the bottom surface of the PM and the top surface of the PCB of 2 mm with the beam in a flat configuration under gravity load. The design parameters for the T-beam FlexLab system are shown in Table I.

The relationship between the magnets' vertical displacements and the Hall effect sensor outputs are calibrated by driving with a M6 screw, and the calibration data of the T-beam FlexLab system is shown in Fig. 9. The position measurement is approximately linear within -1 mm and 1 mm, and becomes noticeably nonlinear when the displacement exceeds this range. When the magnets' motion range is large, 3rd-order polynomial fits can be used to calculate the position of the magnets. Linear fitting is used herein, since in the experiments the magnets' motion is kept within the smaller range. With the calibrated voltage-to-displacement relationship, the estimated position measurement noise standard deviation is 0.2 μm within the 4 kHz controller sampling rate.

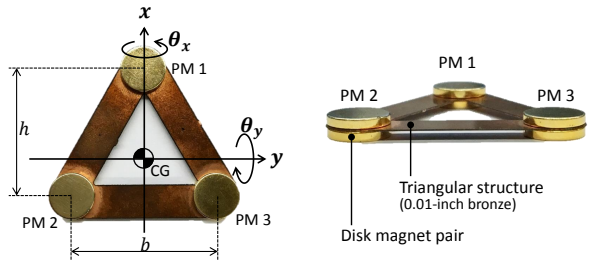

(a) (b)

Fig. 10. Photos of magnetic levitation target for LevLab. (a) Top view with coordinates and magnet distance parameters $h = (\sqrt{3}/2)b$. The coordinate origin is set to the center of gravity. (b) Side view of the LevLab target showing disk magnet pairs.

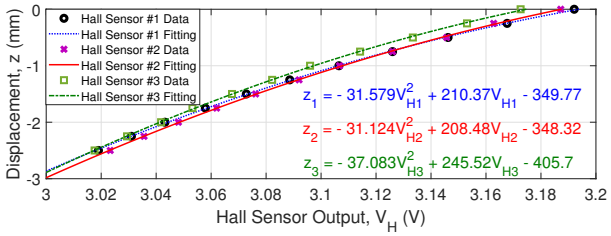

Fig. 11. Levlab configuration calibration data for Hall sensor voltage V_{H_j} as a function of magnet displacement z_j, and as fitted by second order polynomials. In this configuration, the magnet is located below the PC board on the side opposite the Hall cell sensors. The distance scale is defined to be zero when the magnet is in contact with the lower surface of the PC board, and decreases as the magnet moves downward away from the PC board. Calibration is based upon setting the gap between the magnet and PCB via shim stocks with 0.25 mm thickness.

C. Magnetic Levitation System: LevLab

The levitation target of the LevLab is three pairs of disk PMs connected using a water-jet cut 0.01-inch bronze sheet in a triangular shape, as shown in Fig. 10. The Cartesian coordinates used are illustrated in Fig. 10a with the origin set to the center of gravity of the triangular magnet pairs. Note that the levitation direction z is into the paper, which is upward from the PCB board as illustrated in Fig. 14a. The magnet pairs are spaced to be located directly below the actuating coils, resulting in the parameters of $b = 30$ mm and $h = 26$ mm.

The triangular magnet pairs are levitated underneath the actuating coils, as can be seen in Fig. 1b and Fig. 21. Since the magnet locations are different from those in the FlexLab, the Hall sensor output voltages are re-calibrated to the vertical displacements of three magnet pairs. Fig. 11 shows the measured calibration data of three Hall sensors and their second-order polynomial fitting curves. Using the calibrated displacement measurements and the triangular geometry, the target is levitated using a decoupled 3-DOF controller in the translation of z, tilting of θ_x, and tipping of θ_y, as discussed in Section IV-B.

This article has been accepted for publication in a future issue of this journal, but has not been fully edited. Content may change prior to final publication. Citation information: DOI 10.1109/TMECH.2019.2951308, IEEE/ASME Transactions on Mechatronics

III. Modeling and System Identification

This section introduces modeling and system identification for the FlexLab/LevLab. The assumptions of the modeling include:

1) The motion of the magnets is along the vertical direction, and the displacements of the magnets are small;
2) The power amplifiers are linear and have no dynamics;
3) Inductance of the coils are small and has negligible influence to the circuit dynamics;
4) The frequency range considered is limited to be below 100 Hz. As a result, only the first two vibration modes for the T-shaped FlexLab are considered, and the dynamics of the FlexLab system is approximated with lumped parameter mechanical model.

A. Magnetic Force Expression

For the coil configuration, the magnetic force acting on the permanent magnet can be approximated as

$$F = C\frac{i}{z^n}, \tag{1}$$

where z is the vertical distance between the coil and PM, i is the current in the coil, and C and n are constants determined by geometry and magnet parameters [13], [14]. Here the value of n is between 1 and 4. When the distance z is significantly larger than the dimensions of the PM and coil, the magnetic field approaches a dipole interaction, and n approaches 4. When z is small compared with the PM and coil dimensions, the force expression approaches cylindrical-shaped coil interactions, thereby making n close to 1.

In this work, a linearized force expression is used due to the small displacement assumption. Define the steady-state values of z and i as z_0 and i_0, respectively. Linearizing the magnetic force F about the steady-state operating point yields

$$F = \frac{Ci_0}{{z_0}^n} + \frac{C}{{z_0}^n}\delta i - \frac{nCi_0}{{z_0}^{n+1}}\delta z + O(\delta i^2, \delta z^2), \tag{2}$$

where δ denotes the increment of values. Define force constant K_i and negative stiffness K_s as

$$K_i = \frac{C}{{z_0}^n} \quad \text{(N/A)}, \tag{3}$$

$$K_s = -\frac{nCi_0}{{z_0}^{n+1}} \ \text{(N/m)}. \tag{4}$$

Remove δ notation for all variables for conciseness, and define the steady-state force component as F_0, the force expression (2) can then be written as

$$F = F_0 + K_i i + K_s z. \tag{5}$$

The force expression (5) is used in the modeling for the current-force and displacement-force relationships in both the FlexLab and LevLab systems in the following sections. For the FlexLab system, F_0 and K_s equal zero since there is no current in the coil at steady state, i.e. $i_0 = 0$ A.

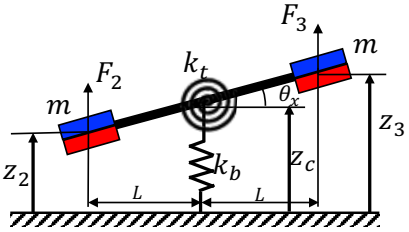

Fig. 12. Lumped two DOF mechanical model with coordinate and geometry definitions for the T-beam FlexLab. The z coordinates are defined to be zero when the magnets are at the centerline of the Hall cells.

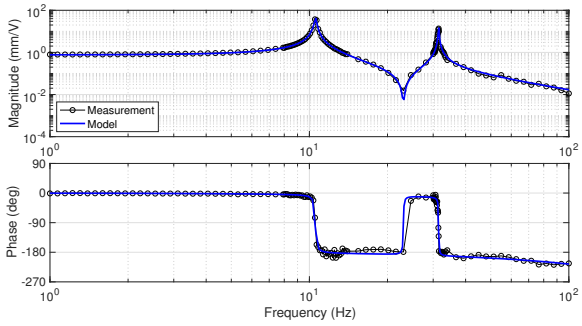

(a)

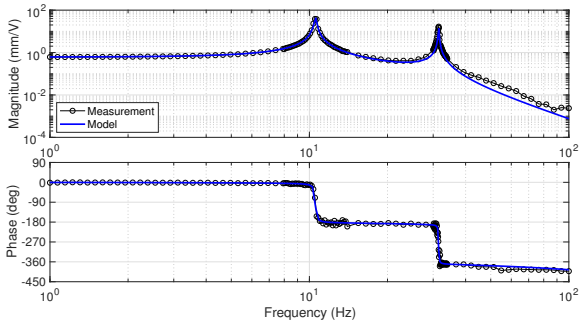

(b)

Fig. 13. Measured and modeled frequency responses of the T-beam FlexLab system driven from coil 2 and measured at sensors 2 and 3.. Note bending and twisting modes at 10 Hz and 32 Hz, respectively. (a) Collocated measurement: $z_2/V_{c2}(j\omega)$. (b) Non-collocated measurement $z_3/V_{c2}(j\omega)$. The data with coil 3 driven is not presented because the system is symmetrical.

For the LevLab system, K_s is non-zero since there is a DC current in the coil to compensate the weight of the target, thereby making the system unstable in open-loop. In the following sections, the values of K_i and K_s are experimentally identified for each system.

B. T-beam FlexLab

The FlexLab system has three different implementations: (a) second-order I-shaped beam system with one pair of PMs, (b) fourth-order T-shaped beam system with two pair of PMs, and (c) sixth-order T-shaped beam system with three pair of PMs. In this section, the modeling and system identification process are presented for the fourth-order T-beam FlexLab system. The other two

This article has been accepted for publication in a future issue of this journal, but has not been fully edited. Content may change prior to final publication. Citation information: DOI 10.1109/TMECH.2019.2951308, IEEE/ASME Transactions on Mechatronics

configurations of FlexLab can be modeled using the same process.

The T-shaped cantilever beam with two PM pairs demonstrates two vibration modes within the considered frequency range: the bending mode and the twisting mode. Since the deformation of the T-shaped beam is concentrated in the longer central section, the bar between the two magnets is assumed to be rigid. Also, since the mass of the connecting bronze bar is much smaller than that of the magnets, the inertia of the bronze connecting bar is neglected. Fig. 12 shows a mechanical element diagram of the T-beam FlexLab system. Here, $m_c = 2m$ is the total mass at the tip of the cantilever beam, $I = 2mL^2$ is the θ_x rotational inertia of the two sets of PMs, k_b and k_t are the bending and twisting stiffnesses of the cantilever beam, respectively, F_2 and F_3 are the magnetic forces on two PMs, z_2 and z_3 are the vertical displacements of the two PMs, $z_c = (z_2+z_3)/2$ is the displacement of the center of mass of the two PM, the distance between the two PMs is $2L$, and θ_x is the angular displacement of the tip of the T-beam about the x-axis. Note that in this model gravity is not included, since the weight of the magnets is balanced with the force provided by the pre-deformed beam at the equilibrium position. The bending and twisting stiffnesses of the beam can be calculated by

$$k_b = \frac{3EI_{beam}}{l_{beam}^3}, \tag{6}$$

$$k_t = \frac{GJ_{beam}}{l_{beam}}, \tag{7}$$

where E and G are the elastic modulus and shear modulus of the beam material, respectively, l_{beam} is the length of the T-beam, I_{beam} is the second moment of area for the T-beam's cross-section, and J_{beam} is the torsional constant for the beam. For a beam with width w and thickness t, $I_{beam} = wt^3/12$, and $J_{beam} = wt^3\big(\frac{1}{3} - 0.21\frac{t}{w}(1 - \frac{t^4}{12w^4})\big)$ [15].

Assuming θ_x is small, we have

$$z_2 = z_c - L\theta_x, \;\; z_3 = z_c + L\theta_x. \tag{8}$$

The dynamic equations for the two vibration modes are

$$m_c\ddot{z}_c + k_b z_c = F_2 + F_3, \tag{9}$$

$$I\ddot{\theta}_x + k_t\theta_x = (F_3 - F_2)L. \tag{10}$$

Substituting (9) and (10) into (8) yields

$$\ddot{z}_2 = \frac{F_2 + F_3}{m_c} - \frac{k_b}{m_c}z_c - \frac{(F_3 - F_2)L^2}{I} + \frac{k_t L}{I}\theta_x, \tag{11}$$

$$\ddot{z}_3 = \frac{F_2 + F_3}{m_c} - \frac{k_b}{m_c}z_c + \frac{(F_3 - F_2)L^2}{I} - \frac{k_t L}{I}\theta_x. \tag{12}$$

Substituting $z_c = (z_2 + z_3)/2$, $\theta_x = (z_3 - z_2)/2L$ and $I = 2mL^2$ into (11) and (12), the equations can be rearranged into matrix form as

$$\begin{bmatrix}\ddot{z}_2\\ \ddot{z}_3\end{bmatrix} = \begin{bmatrix}-\big(\frac{k_t}{2I} + \frac{k_b}{4m}\big) & \big(\frac{k_t}{2I} - \frac{k_b}{4m}\big)\\ \big(\frac{k_t}{2I} - \frac{k_b}{4m}\big) & -\big(\frac{k_t}{2I} + \frac{k_b}{4m}\big)\end{bmatrix}\begin{bmatrix}z_2\\ z_3\end{bmatrix} + \begin{bmatrix}\frac{1}{m} & 0\\ 0 & \frac{1}{m}\end{bmatrix}\begin{bmatrix}F_2\\ F_3\end{bmatrix}. \tag{13}$$

In the next step, the relationship between the coil current i_{c_j} and z_j is obtained using the electrical model in Fig. 14b. Ignoring the coil inductances which have negligible effect for the frequencies of interest, the current in the coil can be written as

$$i_{c_j} = (V_{c_j} - V_{emf_j})/R_c, \tag{14}$$

where $j = 2, 3$ indicates the magnet-coil pair index, R_c is the coil resistance, and V_{emf_j} is the back-electromotive force in the circuit of coil j, which can be calculated by

$$V_{emf_j} = K_i\dot{z}_j. \tag{15}$$

Substituting (14) and (15) into (5), the linearized force between the coil and magnet is

$$F_j = K_i i_{c_j} = \frac{K_i}{R_c}V_{c_j} - \frac{K_i^2}{R_c}\dot{z}_j. \tag{16}$$

Define $\mathbf{x_F} = [z_2, \dot{z}_2, z_3, \dot{z}_3]^\top$, $\mathbf{u_F} = [V_{c_2}, V_{c_3}]^\top$, $\mathbf{y_F} = [z_2, z_3]^\top$. Based on (13)-(16), the state space model for the FlexLab system can be derived as

$$\dot{\mathbf{x_F}} = \mathbf{A_F}\mathbf{x_F} + \mathbf{B_F}\mathbf{u_F}, \tag{17}$$

$$\mathbf{y_F} = \mathbf{C_F}\mathbf{x_F}, \tag{18}$$

where

$$\mathbf{A_F} = \begin{bmatrix}0 & 1 & 0 & 0\\ -\big(\frac{k_t}{2I} + \frac{k_b}{4m}\big) & -\frac{K_i^2}{mR_c} & \big(\frac{k_t}{2I} - \frac{k_b}{4m}\big) & 0\\ 0 & 0 & 0 & 1\\ \big(\frac{k_t}{2I} - \frac{k_b}{4m}\big) & 0 & -\big(\frac{k_t}{2I} + \frac{k_b}{4m}\big) & -\frac{K_i^2}{mR_c}\end{bmatrix},$$

$$\mathbf{B_F} = \begin{bmatrix}0 & 0\\ \frac{K_i}{mR_c} & 0\\ 0 & 0\\ 0 & \frac{K_i}{mR_c}\end{bmatrix}, \mathbf{C_F} = \begin{bmatrix}1 & 0 & 0 & 0\\ 0 & 0 & 1 & 0\end{bmatrix}.$$

The frequency responses of the FlexLab system with the left coil voltage (V_{c_2}) being the input, and displacement of two PMs (z_2 and z_3) being the outputs are measured, as shown in Fig. 13. Note that a higher point density is used in the measurements around the resonance frequencies to better capture the resonances. The frequency response data with the other coil being the input is not presented since the system is symmetrical. The value of K_i in the FlexLab model is identified through comparing the measured and modeled DC gain of the frequency responses. With the identified value $K_i = 0.965$ N/A and other design parameters organized in Table I substituted in, the modeled FlexLab dynamics in (17) and (18) are also plotted together with the measurements in Fig. 13. Note that a 1 ms delay is added in the modeled frequency responses to account for the sampling delay of the myRIO controller. It can be seen that the model and measurements agree well. The system has two resonances within the measured range. The first resonance at 10 Hz corresponds to the bending mode of the beam, while the second resonance at 32 Hz is the twisting mode. Note that an anti-resonance is observed in Fig. 13a at 22 Hz but not in Fig. 13b, which shows the difference between the collocated and non-collocated measurements [16].

This article has been accepted for publication in a future issue of this journal, but has not been fully edited. Content may change prior to final publication. Citation information: DOI 10.1109/TMECH.2019.2951308, IEEE/ASME Transactions on Mechatronics

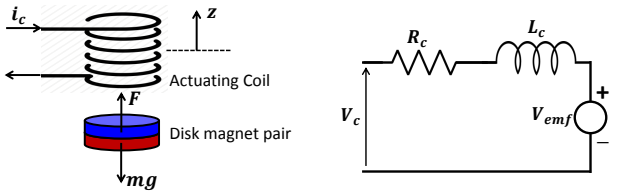

(a) (b)

Fig. 14. Electromechanical model for LevLab magnetic levitation system in each degree of freedom. (a) Mechanical-domain model. (b) Electrical-domain model.

Note that the model did not consider it, but there is a third flexible mode of the FlexLab at 154 Hz, and this resonance frequency sets the limit for the FlexLab position control bandwidth when using.

C. 3-DOF LevLab Modeling

The LevLab system can be modeled as three individual magnet-coil pairs and then decoupled into z, θ_x, and θ_y using the triangular geometry for decoupled 3-DOF levitation control, as discussed in Section IV-B. Fig. 14 schematically shows the electromechanical model of an individual magnet pair interacting with an actuating coil. From the mechanical-domain model in Fig. 14a, an equation of motion is obtained as

$$m\ddot{z}_j = F_j - mg, \tag{19}$$

where j indicates the magnet-coil pair index of 1, 2, and 3. Using the linearized magnetic force on the magnet in (5) and the fact that the steady-state magnetic force F_0 is balanced with the magnet weight mg, we can rewrite (19) as

$$m\ddot{z}_j = K_i i_{c_j} + K_s z_j. \tag{20}$$

From the electrical-domain model in Fig. 14b, the coil current i_{c_j} can be found as (14) under the assumption of negligible coil inductance. Substituting (14) and (15) into (20), the dynamic equation of the single magnet-coil pair is obtained as

$$\ddot{z}_j + \frac{k_i^2}{mR}\dot{z}_j - \frac{K_s}{m}z_j = \frac{K_i}{mR}V_{c_j}. \tag{21}$$

Unlike the FlexLab, we have a negative stiffness term of $-K_s z_j/m$ in the LevLab system due to the need to support the gravity load. Such negative stiffness generates a right half-plane pole, thereby making the system unstable in open-loop. We discuss the stable levitation control of the LevLab system in Section IV-B. Note that in this model the LevLab target is regarded as a rigid body. The control bandwidth of the LevLab system is however limited by the first flexible mode of the system, which is located at 348 Hz.

Using (21) for all three magnet pairs and defining a system state, input, and output respectively as $\mathbf{x_L} = [z_1, \dot{z}_1, z_2, \dot{z}_2, z_3, \dot{z}_3]^\top$, $\mathbf{u_L} = [V_{c_1}, V_{c_2}, V_{c_3}]^\top$, and $\mathbf{y_L} = [z_1, z_2, z_3]^\top$, a state space model of the LevLab system is obtained as

$$\dot{\mathbf{x}}_\mathbf{L} = \mathbf{A_L}\mathbf{x_L} + \mathbf{B_L}\mathbf{u_L}, \tag{22}$$
$$\mathbf{y_L} = \mathbf{C_L}\mathbf{x_L}, \tag{23}$$

where

$$\mathbf{A_L} = \begin{bmatrix} 1 & 0 & 0 & 0 & 0 & 0 \\ -\frac{K_i^2}{mR_c} & \frac{K_s}{m} & 0 & 0 & 0 & 0 \\ 0 & 0 & 1 & 0 & 0 & 0 \\ 0 & 0 & -\frac{K_i^2}{mR_c} & \frac{K_s}{m} & 0 & 0 \\ 0 & 0 & 0 & 0 & 1 & 0 \\ 0 & 0 & 0 & 0 & -\frac{K_i^2}{mR_c} & \frac{K_s}{m} \end{bmatrix},$$

$$\mathbf{B_L} = \begin{bmatrix} 0 & 0 & 0 \\ \frac{K_i}{mR_c} & 0 & 0 \\ 0 & 0 & 0 \\ 0 & \frac{K_i}{mR_c} & 0 \\ 0 & 0 & 0 \\ & 0 & 0\frac{K_i}{mR_c} \end{bmatrix},$$

$$\mathbf{C_L} = \begin{bmatrix} 1 & 0 & 0 & 0 & 0 & 0 \\ 0 & 0 & 1 & 0 & 0 & 0 \\ 0 & 0 & 0 & 0 & 1 & 0 \end{bmatrix}.$$

This model is used to fit a measured frequency response of the z directional levitation to identify the parameters of K_i and K_s. Fig. 19a shows the response of plant model (solid blue curve) fitted onto the measurement (black curve with circle markers) for $K_i = 0.277\,\mathrm{N/A}$ and $K_s = 22.198\,\mathrm{N/m}$. Note that this measurement is taken with the system under closed-loop control, since the system is unstable in open-loop. A delay of 2.4 ms is added to the model to take sampling delay, I/O delay, and other system delays into account, and fit the measured response. During this measurement, the myRIO controller was operating at a sample rate of 4 kHz. We observe a discrepancy in the phase plot with the measured response showing slightly less phase lag around 10 Hz. This is because a copper plate is placed under the levitation target during the frequency response measurements in order to provide additional lateral (x- and y-direction) damping by eddy currents. In the LevLab system, the lateral modes of the levitating target are passively stabilized with relatively low stiffness and damping. When measuring frequency responses using swept sine excitation, the lateral modes can be excited, causing levitation instability. A copper plate is used in order to damp out such lateral vibration by passive eddy current damping, which helped maintain stable levitation during the frequency response measurement process. Such additional eddy current damping resulted in a slight phase lead to all three decoupled DOFs, z, θ_x, and θ_y, as shown in Fig. 19. Note that the copper plate is used only during the frequency-swept measurements, and is not necessary for the closed-loop magnetic levitation in the absence of sinusoidal excitation.

This article has been accepted for publication in a future issue of this journal, but has not been fully edited. Content may change prior to final publication. Citation information: DOI 10.1109/TMECH.2019.2951308, IEEE/ASME Transactions on Mechatronics

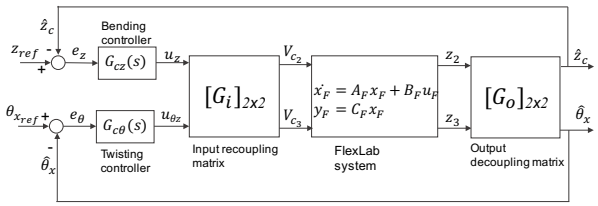

Fig. 15. Block diagram of decoupled control for T-beam FlexLab.

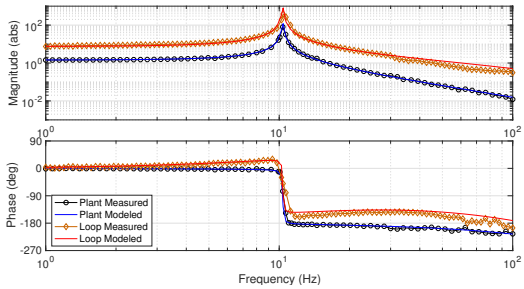

(a)

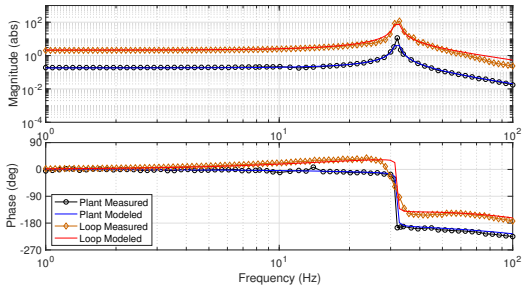

(b)

Fig. 16. Measured and modeled frequency responses of plant and loop for decoupled FlexLab control system. The plant magnitude plots are in units of (mm/V), and the loop magnitude plots are dimensionless. (a) Bending control. (b) Twist control. Note decoupling of the bending and twisting modes.

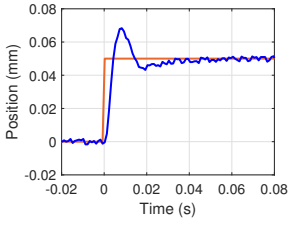

(a)

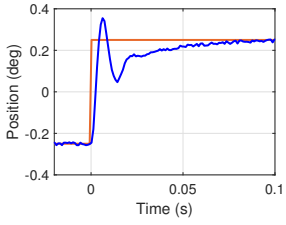

(b)

Fig. 17. FlexLab transient-time responses in closed-loop. Orange line: reference. Blue line: measurement. (a) Bending mode step response. (b) Twisting mode step response.

IV. Controller Design and Performance

A. Position Control of T-beam FlexLab

Fig. 15 shows a block diagram of the control system for the T-beam FlexLab with two PM pairs. The estimated decoupled displacements $\hat{z}_c$ and $\hat{\theta}_x$ are calculated from the measurements by

$$\begin{bmatrix} \hat{z}_c \\ \hat{\theta} \end{bmatrix} = \begin{bmatrix} 1/2 & 1/2 \\ -1/2L & 1/2L \end{bmatrix} \begin{bmatrix} z_2 \\ z_3 \end{bmatrix}. \tag{24}$$

Variables $\hat{z}_c$ and $\hat{\theta}_x$ are then fed back and compared with their reference values, and the error signals are fed into controllers G_{cz} and $G_{c\theta}$. The control effort signals corresponds to the bending control voltage u_z and twisting control voltage u_{θ_z}, respectively. These signals are transformed back to the coupled coordinate by

$$\begin{bmatrix} V_{c_2} \\ V_{c_3} \end{bmatrix} = \begin{bmatrix} 1/2 & -1/2L \\ 1/2 & 1/2L \end{bmatrix} \begin{bmatrix} u_z \\ u_{\theta_x} \end{bmatrix}. \tag{25}$$

Finally the coil voltage commands V_{c_2} and V_{c_3} are sent to the amplifiers and energize the coils.

The control loop shown in Fig. 15 is experimentally implemented for the FlexLab system. Here, the two controllers are designed as

$$G_{cz}(s) = K_z \frac{\alpha\tau_z s + 1}{\tau_z s + 1}, \tag{26}$$

$$G_{c\theta}(s) = K_\theta \frac{\alpha\tau_\theta s + 1}{\tau_\theta s + 1}, \tag{27}$$

where $\alpha = 10$, $K_z = 3.2$ V/mm, $K_\theta = 6.6$ V/deg, $\tau_z = 1 \times 10^{-3}$ s, $\tau_\theta = 7.75 \times 10^{-4}$ s. Fig. 16 shows the measured frequency responses of the decoupled T-beam FlexLab control system, with Fig. 16a showing the response of the bending control loop, and Fig. 16b for the twisting control loop. Both modeled and measured responses show well-decoupled modes, bending at 10 Hz and twisting at 32 Hz, of the FlexLab, as compared to the coupled responses in Fig. 13. The cross-over frequencies of the bending and twisting control loops are 50 Hz and 65 Hz, respectively, and both control loops demonstrate a phase margin of about 45 degrees. Fig. 17 shows the measured step responses of the bending and twisting modes of the FlexLab system. The step responses show consistent bandwidth with the frequency response measurement in Fig. 16.

B. Levitation Control of 3-DOF Magnets

Fig. 18 shows the schematic block diagram of the 3-DOF decoupled levitation control for the LevLab system. The decoupled DOFs are estimated using the calibrated magnet displacement z_j and the triangular geometry of the levitation target, resulting in a matrix relation of

$$\begin{bmatrix} \hat{z} \\ \hat{\theta}_x \\ \hat{\theta}_y \end{bmatrix} = \begin{bmatrix} 1/3 & 1/3 & 1/3 \\ 0 & -1/b & 1/b \\ -1/h & 1/2h & 1/2h \end{bmatrix} \begin{bmatrix} z_1 \\ z_2 \\ z_3 \end{bmatrix} = \mathbf{T_o} \begin{bmatrix} z_1 \\ z_2 \\ z_3 \end{bmatrix}, \tag{28}$$

where $\mathbf{T_o}$ is the 3×3 output decoupling matrix. These estimated decoupled displacements are fed back to close the control loop with a 3×3 diagonal lead controller matrix $\mathbf{C_{lead}}(s)$, stabilizing the magnetic levitation system. Note that the real-time levitation control loop runs deterministically at 4 kHz. The control effort voltages, u_z, u_{θ_x}, and u_{θ_y} are then re-coupled to provide the required voltage to each actuating coil using the matrix relation of

$$\begin{bmatrix} V_{c_1} \\ V_{c_2} \\ V_{c_3} \end{bmatrix} = \begin{bmatrix} 1/3 & 0 & -1/h \\ 1/3 & -1/b & 1/2h \\ 1/3 & 1/b & 1/2h \end{bmatrix} \begin{bmatrix} u_z \\ u_{\theta_x} \\ u_{\theta_y} \end{bmatrix} = \mathbf{T_i} \begin{bmatrix} u_z \\ u_{\theta_x} \\ u_{\theta_y} \end{bmatrix}, \tag{29}$$

This article has been accepted for publication in a future issue of this journal, but has not been fully edited. Content may change prior to final publication. Citation information: DOI 10.1109/TMECH.2019.2951308, IEEE/ASME Transactions on Mechatronics

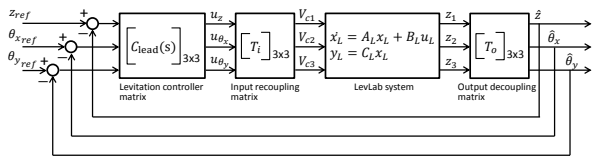

Fig. 18. Block diagram of decoupled 3-DOF magnetic levitation for LevLab with the state space model as a plant, 3×3 diagonal control matrix ($\mathbf{C_{lead}}$(s)), and 3×3 coordinate conversion matrices ($\mathbf{T_i}$ and $\mathbf{T_o}$).

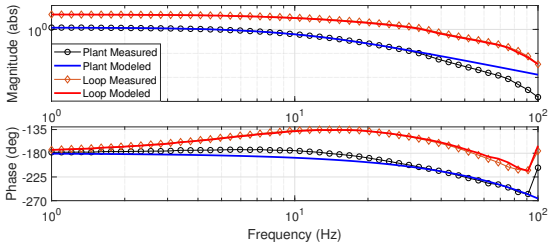

(a)

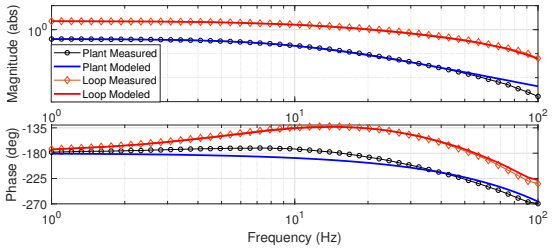

(b)

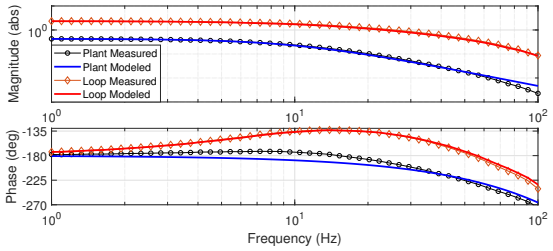

(c)

Fig. 19. Measured and modeled frequency responses of plant and loop for three decoupled levitation DOFs. The plant magnitude plots are in units of (mm/V) for z and (deg/V) for θ_x and θ_y while the loop magnitude plots are dimensionless. (a) z-direction. (b) θ_x-direction. (c) θ_y-direction.

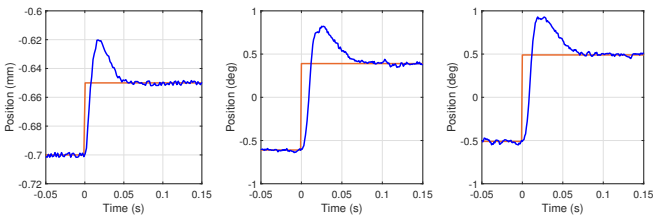

(a) (b) (c)

Fig. 20. Measured step responses of the LevLab system under closed-loop control. Orange line: reference. Blue line: measurement. (a) z-direction. (b) θ_x-direction. (c) θ_y-direction.

where $\mathbf{T_i}$ is the 3×3 input recoupling matrix. The controller matrix used is a 3×3 diagonal matrix consisting of lead compensators to stabilize the three decoupled

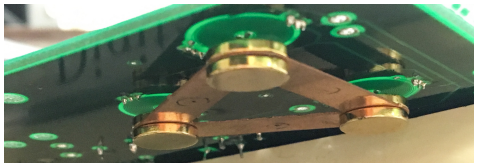

Fig. 21. Photo of 3-DOF decoupled magnetic levitation of LevLab with 0.7 mm levitation gap.

levitation DOFs, and is written as

$$\mathbf{C_{lead}}(s) = \begin{bmatrix} K_z \frac{\alpha\tau s+1}{\tau s+1} & 0 & 0 \\ 0 & K_{\theta_x} \frac{\alpha\tau s+1}{\tau s+1} & 0 \\ 0 & 0 & K_{\theta_y} \frac{\alpha\tau s+1}{\tau s+1} \end{bmatrix}. \quad (30)$$

Fig. 19 shows the measured decoupled loop return ratios of all three levitation DOFs using the controller parameters of $\alpha = 10$, $\tau = 2 \times 10^{-3}$ s, $K_z = 1.8$ V/mm, $K_{\theta_x} = 5.3$ V/deg, and $K_{\theta_x} = 4.9$ V/deg. The decoupled 3-DOF levitation is stabilized with the transitional (z) levitation loop having a crossover frequency of about 30 Hz with the phase margin of 30° while both the tip (θ_y) and tilt (θ_x) levitation loops cross over at 20 Hz with 45° phase margin. Fig. 20 shows the measured closed-loop step responses of the LevLab in the three actively-controlled DOFs. The step response data are consistent with the frequency response measurements shown in Fig. 19.

A stable 3-DOF magnetic levitation is performed using the LevLab system, as shown in Fig. 1b and Fig. 21. The levitation gap is set to 0.7 mm and the tip and tilt are referenced to zero. A DC voltage offset of 3.1 V is used for each actuating coil to compensate the weight of levitating magnet pairs, resulting in a DC current of 0.3 A and associated power consumption of 0.9 W per coil. The temperature of the coils rise to 30 °C at steady-state.

V. Teaching Applications

The FlexLab/LevLab system can be used for teaching at three different levels: (1) introductory-level dynamic systems and control class for early undergraduate students, (2) mid-level control class for more senior undergraduate students, and (3) advanced-level control and mechatronics class for graduate students. It is suggested to supply students with one real-time microcontroller and one FlexLab/LevLab system during the lab assignment, which allows students to interact with the hardware outside class time. This section discusses the suggested lab assignment tasks using the FlexLab/LevLab system in classes of different levels.

A. Introductory Class

In an introductory dynamics and control class, the second-order (1-DOF) FlexLab system using an I-shaped cantilever beam (as shown in Fig. 7) is suggested. The lab assignment tasks can include: (1) model the I-shaped cantilever beam as a second-order mass-spring-damper system, (2) measure the time and frequency responses of

the I-beam FlexLab, (3) identify model parameters including the natural frequency and damping ratio from the measured responses, and (4) design and test a controller for the system via loop-shaping techniques. Through such a series of lab tasks, students can observe the dynamics of a second-order mechanical system, practice loop-shaping controller design, and test the feedback control experimentally.

B. Mid-level Undergraduate Class

In a mid-level control class for undergraduate students, the fourth-order (2-DOF) T-beam FlexLab system (as shown in Fig. 8) is suggested. The detailed tasks in the lab assignment using the T-beam FlexLab can include: (1) model the FlexLab T-beam system considering both the mechanical and electrical domains, (2) calibrate the sensors and actuators, and (3) identify the system dynamics via time and frequency responses. Through these lab assignments, students can learn about the modeling for multi-input-multi-output (MIMO) systems, observe collocated and non-collocated system dynamics, and understand the physical meaning of complex zeros, as shown by the anti-resonance in Fig. 13a.

C. Advanced-level Class

Both the FlexLab and LevLab systems can be utilized for the development of an advanced-level control and mechatronics class for graduate students. For the 2 DOF T-beam FlexLab system, aside from modeling and system identification, additional tasks can be given to students including: (1) design input and output decoupling matrices, (2) shape the loop return ratios of the decoupled systems to close the position loops in 2 DOF, and (3) experimentally demonstrate the closed-loop control performance. The 1-DOF and 3-DOF LevLab systems are also suggested for teaching an advanced-level class, through which students can explore the behavior of dynamic systems that are unstable in open-loop. They can learn how to design controllers to stabilize open-loop unstable systems using feedback control techniques. As a further study, it is considered to use the FlexLab/LevLab system to teach the state-space method of modeling and controller design for multi-input-multi-output systems.

VI. Conclusions and Future Work

This paper has described the new FlexLab/LevLab system which implements a number of possible electromechanical mechatronics experiments on a single PC board. This device is sufficiently portable and low-cost to allow students to borrow these during a course so as to be able to accomplish experimental work outside a traditional lab setting. The FlexLab/LevLab implements systems as simple as a second-order spring/mass/damper, as well as higher-order MIMO electromechanical systems, including distributed modes. A number of magnetic levitation experiments are also possible with this device. Analytical models for some example systems are presented and are compared with experimental measurements. Experimental results are also shown for decoupling control of the flexible beam system of two degrees of freedom and the magnetic levitation system with three degrees of freedom. Thus the system supports experiments from basic second-order dynamics as might be taught at the sophomore level to MIMO control of a system with distributed modes or freely levitating devices which might be the subject of more advanced courses. The design files, example control code, and operating videos of the FlexLab/LevLab system are available for download at *https://pmc.mit.edu/projects/project-flexlab-and-levlab*.

The FlexLab has been used at MIT as a platform for the final project of *2.14/2.140 Analysis and Design of Feedback Control Systems* in Spring, 2018. With the FlexLab system, the students can observe collocated and non-collocated system dynamics, understand the physical meaning of complex zeros, and learn decoupled control for a MIMO system. We plan to continue to use this device in future semesters to allow students to explore other aspects of the dynamics and control of mechatronic systems.

Suggested future work includes: (1) the use of the FlexLab/LevLab system with alternative real-time microcontrollers, (2) the use of the FlexLab/LevLab system for teaching state-space controller design methods including using optimal control approaches, and (3) the design of educational magnetic suspension system with the target levitated on top of the actuators, as presented in [17] with one possible configuration.

Acknowledgment

The authors would like to thank the Department of Mechanical Engineering at MIT as well as National Instruments company for supporting this work.

References

[1] M. Raab, A. Kazi, and D. L. Trumper, "Magnetically levitated bldc motor as a modular teaching tool," in *Research and Education in Mechatronics (REM), 2015 16th International Conference on*. IEEE, 2015, pp. 255–262.

[2] F. Ghorbel and J. B. Dabney, "A spherical pendulum system to teach key concepts in kinematics, dynamics, control, and simulation," *IEEE Transactions on Education*, vol. 42, no. 4, pp. 2–pp, 1999.

[3] J. G. Cham, B. Stafford, and M. R. Cutkosky, "See labs run: A design-oriented laboratory for teaching dynamic systems," in *ASME, IMECE*, 2001, pp. 11–16.

[4] A. M. Okamura, C. Richard, M. Cutkosky *et al.*, "Feeling is believing: Using a force-feedback joystick to teach dynamic systems," *Journal of Engineering Education*, vol. 91, no. 3, pp. 345–349, 2002.

[5] Y. Xie, "Mechatronics examples for teaching modeling, dynamics, and control," Master's thesis, Massachusetts Institute of Technology, 2003.

[6] R. M. Reck and R. S. Sreenivas, "Developing a new affordable dc motor laboratory kit for an existing undergraduate controls course," in *American Control Conference (ACC), 2015*. IEEE, 2015, pp. 2801–2806.

[7] J. P. Oliver and F. Haim, "Lab at home: Hardware kits for a digital design lab," *IEEE Transactions on Education*, vol. 52, no. 1, pp. 46–51, 2009.

[8] J. Sarik and I. Kymissis, "Lab kits using the arduino prototyping platform," in *Frontiers in Education Conference (FIE), 2010 IEEE*. IEEE, 2010, pp. T3C–1.

[9] "NI myRIO Hardware at a Glance," National Instruments, Tech. Rep., 08 2014.
[10] V. H. Nguyen and W.-j. Kim, "Two-phase lorentz coils and linear halbach array for multiaxis precision-positioning stages with magnetic levitation," *IEEE/ASME Transactions on Mechatronics*, vol. 22, no. 6, pp. 2662–2672, 2017.
[11] H. Zhu, T. J. Teo, and C. K. Pang, "Design and modeling of a six-degree-of-freedom magnetically levitated positioner using square coils and 1-d halbach arrays," *IEEE Transactions on Industrial Electronics*, vol. 64, no. 1, pp. 440–450, 2016.
[12] On semiconductors, *1.0 A Output Current, Dual Power Operational Amplifiers*. TCA0372 Datasheet, 2013.
[13] H. A. Haus and J. R. Melcher, *Electromagnetic fields and energy*. Prentice Hall, 1989.
[14] D. Vokoun, M. Beleggia, L. Heller, and P. Šittner, "Magnetostatic interactions and forces between cylindrical permanent magnets," *Journal of magnetism and Magnetic Materials*, vol. 321, no. 22, pp. 3758–3763, 2009.
[15] D. Johnson, *Advanced structural mechanics: an introduction to continuum mechanics and structural dynamics*. Collins, 1986.
[16] R. M. Schmidt, G. Schitter, and A. Rankers, *The Design of High Performance Mechatronics-: High-Tech Functionality by Multidisciplinary System Integration*. Ios Press, 2014.
[17] A. Gohin, J. Simeray, W. Bing, and L. Qing, "Levitation device," Jul. 26 2007, uS Patent App. 11/592,464.

Lei Zhou (SM'16) received the M.S. and Ph.D. degrees in Mechanical Engineering from Massachusetts Institute of Technology, Cambridge, MA, USA, in 2014 and 2019, respectively, and received the B.E. degree in Control and Instrumentation Engineering from Tsinghua University, Beijing, China in 2012. Her research is in the field of precision mechatronics, with an emphasis on electromagnetic design, actuators and sensors, precision control, and magnetic suspension.

Jun Young Yoon received the B.S. degree in mechanical engineering from Yonsei University, Seoul, Korea, in 2009 and the M.S. and Ph.D degrees in mechanical engineering from Massachusetts Institute of Technology, Cambridge, MA, USA, in 2011 and 2017, respectively. He is currently an Assistant Professor at the School of Mechanical Engineering, Yonsei University. He was a postdoctoral researcher in mechanical engineering at Massachusetts Institute of Technology for two years from 2017. His current research interests include manufacturing mechatronics and robotics system design, electromagnetic and electromechanical machine design, mechatronic device design and control for microphysiological systems such as organs-on-chips, friction microdynamics modeling and compensation, and precision motion control.

Alex Andriën received the B.Sc. degree in Mechanical Engineering and the M.Sc. degree in Systems and Control at the Eindhoven University of Technology (TU/e) in the Netherlands in 2013 and 2016, respectively. He is currently pursuing the Ph.D. degree in the Control Systems Technology group within the department of Mechanical Engineering at the TU/e. His current research interests include machine learning, control systems, robotics and unmanned aerial vehicles.

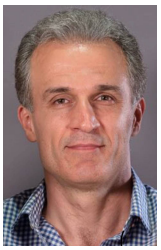

Mohammad Imani Nejad received his Ph.D. in Mechanical engineering from MIT, Cambridge, MA, USA in 2013 with focus on Bearingless motors. He is the founder of IIMANII, Inc., working on various electric motors and generators for aviation application including hybrid systems for multi-copters. He is also working on linear motors for high precision systems.

Blair T. Allison is a professor of Mechanical Engineering at Grove City College. Prior to joining Grove City College in 1999, he worked fifteen years for Alcoa, Inc. in the areas of rolling mill control, metal forming process control, and extrusion forming process and equipment development for automotive applications. His time with Alcoa also included a two-year assignment in Soest, Germany during the startup phase of a facility that manufactured automotive components for Audi AG. He currently teaches courses in system dynamics and control, robotics, mechanics of materials, materials science, and finite element analysis. Areas of research interest include the modeling and control of metal forming processes, manufacturing automation and control, and mechatronics. He received his Ph.D. and M.S. degrees in mechanical engineering from the Massachusetts Institute of Technology and his B.S.M.E. degree from Carnegie Mellon University.

David L. Trumper (M'90) joined the MIT Department of Mechanical Engineering in August 1993, and holds the rank of Professor. He received the B.S., M.S., and Ph.D. degrees from MIT in Electrical Engineering and Computer Science, in 1980, 1984, and 1990, respectively. Following the Bachelor's degree, Professor Trumper worked two years for the Hewlett-Packard Co. After finishing the Master's degree, he worked for two years for the Waters Chromatography Division of Millipore. Upon completing the Ph.D. degree, for three years he was an Assistant Professor in the Electrical Engineering Department at the University of North Carolina at Charlotte, working within the precision engineering group. Professor Trumper's research centers on the design of precision mechatronic systems, with a focus on the design of novel mechanisms, actuators, sensors, and control systems. He has conducted research in topics including precision motion control, high-performance manufacturing equipment, novel measurement instruments, biomedical and bio-instrumentation devices, and high-precision magnetic suspensions and bearings. He is a member of the IEEE, ASME, and ASPE (past-President).